INSTITUTE OF PHYSICS PUBLISHING MEASUREMENT SCIENCE AND TECHNOLOGY

Meas. Sci. Technol. **14** (2003) 251–259 PII: S0957-0233(03)35135-5

Transient thermal response of a hot-wire anemometer

S C Morris[1] **and J F Foss**

Department of Mechanical Engineering, Michigan State University, East Lansing, MI 48824, USA

Received 22 March 2002, in final form and accepted for publication 20 November 2002
Published 3 February 2003
Online at stacks.iop.org/MST/14/251

Abstract

The ability of a thermal anemometry system to accurately measure unsteady fluid velocity depends on the electrical control system as well as the thermal properties of the sensor. The present work is a numerical study of the thermal transient response of a hot-wire. A conventional constant temperature anemometer with an ideal feedback amplifier as well as a pulse width modulated system were used to model the electrical current supplied to the sensor to maintain a nominally constant sensor resistance. The agreement between these two electrical models confirmed that the response characteristics are only due to thermal effects. The thermal response was tested by providing a known input function for the cooling velocity, and comparing this with the output of the model. The first test used a step input function. It was found that the thermal transient effects along the length of the sensor caused the system to initially under predict the actual velocity increase; this was followed by an exponential increase to the steady state velocity. Secondly, the model was tested with sinusoidal inputs over a wide frequency range. The ratio: indicated-velocity/input-velocity, as a function of the input frequency was used to characterize the 'thermal frequency response'.

Keywords: hot-wire anemometry, computational heat transfer, thermal frequency response

(Some figures in this article are in colour only in the electronic version)

Nomenclature

A_c	cross sectional area of the sensor
A, B, n	calibration coefficients
c	specific heat
C-CTA	conventional constant temperature anemometer
D_{Co}	copper plating diameter
D_{Tu}	tungsten sensor diameter
E	voltage
f	frequency of sine wave input to model
f^*	dimensionless frequency of velocity input function
I	electrical current
k	thermal conductivity
q_{axial}	heat transfer along the sensor
q_{radial}	heat transfer from the sensor to the fluid
L	length of the sensor
Nu	Nusselt number
Pr	Prandtl number
PWM	pulse width modulated CTA
R	electrical resistance
Re	Reynolds number
$\langle T \rangle$	clock time for the PWM circuit
T'	heating cycle time for PWM
t	time
t_0	time location of step function (see equation (11))

[1] Current address: Department of Aerospace and Mechanical Engineering, University of Notre Dame, USA.

 © 2003 IOP Publishing Ltd Printed in the UK

t_f	response time of C-CTA
$T(x,t)$	wire temperature
V	cooling velocity of the fluid
x	coordinate along the sensor axis
α	thermal diffusivity
ϕ	response ratio of sensor
$\tau_{thermal}$	time constant of analytical solution (equation (14))
τ	duration of heating current of a PWM cycle
ρ	density of sensor material
Subscripts	
n	spatial node
k	pulse number of PWM-CTA
f	indicates properties evaluated at film temperature
Superscript	
p	simulation time step

1. Introduction

Constant temperature anemometry (CTA) has been used for the measurement of velocity and wall shear stress in turbulent flow fields for nominally four decades; see Bruun (1995). This technique typically utilizes a hot-wire or hot film sensor which is heated to a constant temperature using an electronic control system. This control system, along with the thermal transient effects within the sensor will control the dynamic response of the system. The effects of the electronic control have been studied by, for example, Freymuth (1977) and Perry (1982). However, the frequency response characteristics of the sensor due to thermal effects have not been thoroughly established. The present study will provide quantitative information about the thermal frequency response of a typical hot-wire sensor using a finite element heat transfer calculation.

A schematic representation of a typical sensor is shown in figure 1. The temperature of the sensor is maintained at a nominally constant value of $1.7T_{gas}$, where 1.7 is the heating ratio. The electronic control system establishes the average temperature of the sensor by maintaining the operating resistance of the sensor at the level: $R_{hot} = 1.7R_{cold}$. Note that it is the net resistance, and hence the spatial *average* operating temperature of the sensor, which is controlled. For a given sensor geometry, the steady state temperature distribution is a function of the cooling velocity; see figure 2. These temperature distributions are derived analytically for the steady state case in Freymuth (1979). The two curves represent $T(x)$ for a high and low cooling velocity. The differences between the curves have been exaggerated for illustrative purposes.

The importance of these temperature distributions becomes evident when considering the energy balance for the sensor:

electrical input power = convection to fluid

+ conduction to supports. (1)

The electrical power supplied to the sensor is measured as the square of the output voltage from the anemometer. The convective heat transfer is related to the fluid velocity by the $Nu = Nu(Re)$ relationship, where Nu is the Nusselt number and Re is the Reynolds number for the steady state flow past the sensor. In addition, the conductive heat transfer

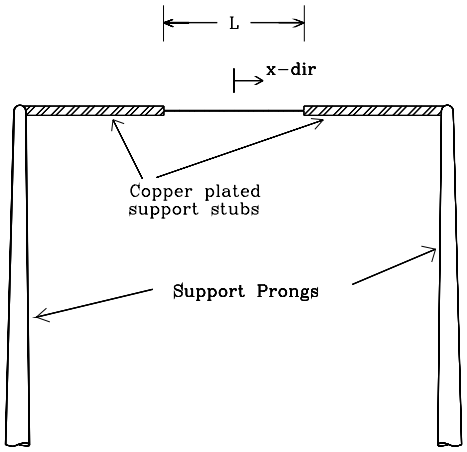

Figure 1. Schematic of the simulated hot-wire sensor.

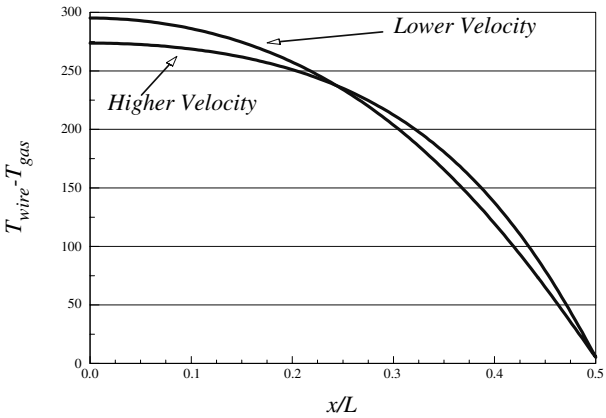

Figure 2. Schematic of temperature distribution at high and low cooling velocities. Note that the difference in temperature has been exaggerated for illustrative purposes. Actual temperature differences are given in figure 13.

to the support stubs also depends on the magnitude of the fluid velocity. Specifically, the conduction is given by the temperature gradient at $(x = L/2)$. Because the distribution $T(x)$ is dependent on the fluid velocity as shown in figure 2, the conduction can also be considered a function of the fluid velocity.

In steady state operation, these effects are accounted for in the calibration procedure which relates the cooling velocity to the anemometer's output; that is, the right and left sides of equation (1), respectively. However, because the thermal transient effects within the sensor will occur with a much longer time constant than that of the sensor control system, the steady state relationship provided by the calibration will not accurately represent the conduction term at $x = L/2$ if rapid velocity changes are present. These effects, which will be described more thoroughly and quantitatively in the results section, represent the focus of this communication.

Previous efforts which have described these thermal effects include Perry (1982). In chapter 2 of this reference, the combination of electrical and thermal effects were written as a differential equation (2.8.2) to model the appropriate heating and cooling terms. A time-averaged and a linear perturbation of this equation were derived. These equations and their boundary conditions were solved to provide a relationship

between a perturbation in velocity or gas temperature to the resulting perturbation in wire voltage. The complexity of these solutions, however, prevents easily obtained quantitative conclusions about the interpretation of anemometry data from turbulent flow fields.

The effect of thermal transients on the frequency response of the sensor was also studied analytically by Freymuth (1979). His equations describe a critical frequency: f_ℓ, above which the sensor response is reduced to a nominally constant value: ε_ℓ. The theory provides estimates of ε_ℓ and f_ℓ based on the material properties and geometry of the sensor. Freymuth then provides a qualitative representation of the shape of the frequency response curve based on these parameters. The present numerical work supports these findings and provides quantitative results without the use of the assumptions which were required for the analytical findings; see section 4.3 of the present communication. It is noteworthy that the present computations support Freymuth's theory and that, in the judgement of the present authors, these theoretical considerations have not been adequately recognized. For example, this important aspect of thermal anemometry is not considered in the monograph by Bruun (1995) nor in the handbook chapter by Comte-Bellot (1998).

The following section presents the details of the heat transfer model that was used in the calculation. Since the present objective was to isolate the sensor effects from the electrical characteristics, two separate electrical circuits were modelled to validate this isolation: an idealized conventional (C-CTA), and a pulse-width-modulated (PWM-CTA) anemometer. Section 3 presents the electrical control system models for these two circuits. Agreement from these two types of anemometer circuit simulations confirms that the response is solely a function of the sensor element.

Section 4 describes the results of the calculation for varied input cooling velocity functions. The relationship between the input velocity and the output of the simulated anemometer was obtained using steady state input velocities. These results were used to 'calibrate' the model in a similar way that a physical calibration would be used. Secondly, a step function was used to provide an understanding of the heat transfer balance after a sudden change in cooling velocity. Lastly, a series of sinusoidal inputs were used to create a plot of the thermal frequency response.

2. Thermal model of sensor

A wide variety of hot-wire materials and geometries are utilized in the measurement of fluid velocities. A typical hot-wire probe used in gas phase turbulence research was chosen for the present computations; see figure 1. This hot-wire uses a 1 mm active region of 5 μm tungsten filament with 50 μm copper plated support stubs, as recommended by Comte-Bellot (1976). The unplated tungsten is referred to as the 'active' portion of the sensor. The x-coordinate for the sensor is shown from the centre of the wire.

Figure 3 shows a detailed view of the sensor model. Both the tungsten and copper sections were discretized in the x direction; lumped capacitance was assumed in the radial direction since the Biot number in the radial direction is quite small; $Bi \approx 10^{-4} \ll 1$, see Incropera and DeWitt (1990). The

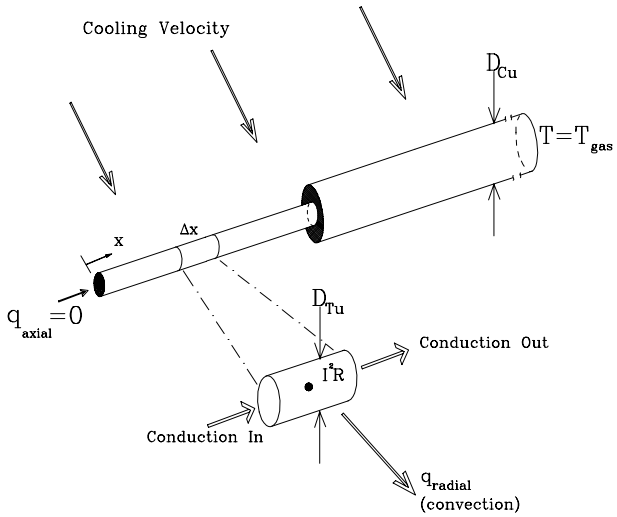

Figure 3. Modelled hot-wire with boundary conditions (not to scale). The Δx segment represents one of the 165 nodes identified in the equations of section 2.1.

half-sensor was discretized with 150 nodes ($n = 1, \ldots, 150$) in the tungsten and 15 nodes ($n = 151, \ldots, 165$) in the copper stub, where n denotes the node number. It was found that additional nodes changed the results less than 0.1%.

2.1. Governing equations

The differential equation governing the transport of thermal energy is given by:

$$\rho c A_c(\Delta x)\frac{\partial T}{\partial t} = q_{axial} + q_{radial} + I^2 R. \tag{2}$$

The left-hand side represents the time rate of change of thermal energy of a single element (Δx). The terms of the right-hand side represent the net conduction, convective cooling, and volumetric heating, respectively, for a given element. The time derivative was discretized using a simple forward difference:

$$\rho c A_c(\Delta x)\frac{\partial T}{\partial t} = \rho_n c_n (A_c)(\Delta x)\frac{T_n^{p+1} - T_n^p}{\Delta t}. \tag{3}$$

The subscript 'n' indicates that these property values were evaluated at each node to account for their variations with temperature. The conductive heat transfer along the length of the sensor (q_{axial}) was modelled with a second order spatial difference:

$$q_{axial} = k_n A_c(\Delta x)\left(\frac{\partial^2 T}{\partial x^2}\right) = k_n A_c\left(\frac{T_{n+1}^{p+1} + T_{n-1}^{p+1} - 2T_n^{p+1}}{\Delta x}\right). \tag{4}$$

The radial heat flux (convection) from each segment of the sensor, as well as that of the plated section, was modelled by the Nusselt number relation:

$$Nu = 0.42 Pr_f^{0.26} + 0.57 Pr_f^{0.33} Re_f^{0.45}. \tag{5}$$

This $Nu = f(Re, Pr)$ relationship, is given by Bruun (1995). Note that the subscript (f) indicates that all fluid properties are evaluated at the 'film temperature', where $T_{film} = (T_{wire} - T_{ambient})/2$. Although the form of equation (5) is consistent in

the literature, the constants used vary, see, e.g., Perry (1982). The results of the present simulation will not be sensitive to the specific $Nu = f(Re, Pr)$ relationship since the anemometer's response is numerically 'calibrated' as described in section 4.1.

The Joule heating term was calculated for each node as:

$$I^2 R_n = \left(\frac{E_{sensor}}{R_{sensor}}\right)^2 R_n \tag{6}$$

where E_{sensor} is the voltage across the simulated probe by the electronic control circuit (see section 3), and R_{sensor} is the total resistance of the probe.

2.2. Boundary conditions

The velocity vector was considered to be perpendicular to the sensor. Hence symmetry permits the model to be applied to half of the sensor. The boundary condition at the half plane ($x = 0$) was that of zero axial heat conduction:

$$\left.\frac{\partial T}{\partial x}\right|_{x=0} = 0. \tag{7}$$

The interface between the tungsten and copper sections ($x = L/2$) was treated as an abrupt change in material and diameter. Note that this is in contrast to that used in Perry (1982) where the copper plating was assumed to taper down gradually. Environmental scanning electron microscope (ESEM) photos of probes manufactured by the authors have shown that the abrupt change in diameter provides a good description of our probes.

The boundary condition at the end of the copper plating: $T = T_{gas}$ was considered to be rational given the relatively large thermal mass of the support prongs.

2.3. Steady state temperature solution

The boundary conditions and equation (2) for each node created a set of 165 coupled algebraic equations. A tri-diagonal matrix of the coefficients was created and inverted to solve for the new temperature distribution at each time step. The implicit nature of the conduction solution ensures numerical stability.

The temperature distribution for a steady state input velocity of 7.5 m s^{-1} and an overheat ratio $R_{hot}/R_{cold} = 1.7$ is shown in figure 4. The zero temperature gradient at $x = 0$ is evident. Also note the strong heat sink effect of the copper plating. The temperature at the end of the sensor was $T(L/2) - T_{gas} = 13.2\,^{\circ}$C compared to the mean wire temperature of 210 °C above ambient. An important feature of this solution is that the effect of conduction to the supports has propagated throughout the length of the sensor. The steady state temperature solution was solved analytically (see Freymuth 1979) and is shown along with the numerical solution on figure 4. The agreement indicates that the spatial resolution of the discrete model (150 tungsten nodes, 15 copper nodes) is sufficient.

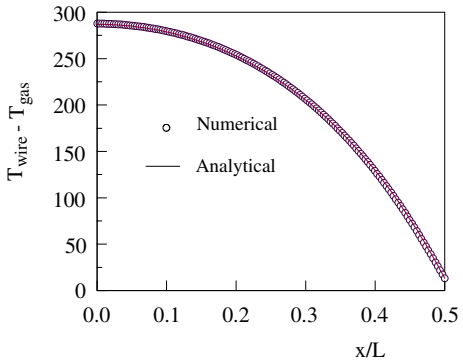

Figure 4. Steady state temperature distribution.

3. CTA models

The thermal model described in section 2 was used with two types of modelled CTA electronic circuits. The term 'conventional' is used to refer to a Weatstone bridge-feedback amplifier type of system. This will be described in section 3.1. The recently developed 'PWM' (see Foss *et al* 1996) electronic control was also simulated. This system provides several advantages over a conventional system as described in section 3.2.

3.1. The conventional CTA

The parameters of the simulated electrical components were chosen to have nearly ideal operating characteristics in order to isolate the thermal effects from the electrical control model. For example, an unrealistically large gain-bandwidth specification was used to represent the amplifier. The modelled components were also considerably less complex than those used in a physical device. For example probe cable effects were not considered.

The Wheatstone bridge and amplifier of the conventional CTA (C-CTA) are shown schematically in figure 5. The equations used to model the curcuit can be found in any standard reference, for example, Thomas and Rosa (2001). The amplifier was modelled as a single pole filter with a gain of 49 000 and a corner frequency of 5 MHz. Note that the gain-bandwidth product of this hypothetical amplifier was 2.5×10^{11} Hz, compared to a physical device in which a value of order 5×10^7 Hz is typical. The circuit model was used to compute the electrical voltage to be supplied to the wire model in equation (6) at each time step. The time discretization of the model was set to $\Delta t = 15.6$ ns. These data were then resampled at 64 000 Hz for storage which corresponds to the operating frequency of the PWM-CTA simulation discussed in the next section.

The response of the modelled system was tested using a square wave perturbation in the feedback amplifier. This test, in which a 50 mV step was applied to the sensor operating at a steady state 7.5 m s^{-1} input velocity, is the same as that used in physical systems. The voltage response function is shown in figure 6. This output can be characterized as a slightly underdamped response with a 13% overshoot. The time of the first crossing of the steady state value was $t_c = 0.2\ \mu$s. Hence the effective frequency response of the simulated anemometer was estimated to be (see Freymuth 1977):

$$f = \frac{1}{1.3t_c} = 3.8 \times 10^6 \text{ Hz}. \tag{8}$$

These characteristics represent a nearly ideal anemometer that could not be physically realized given the limitations

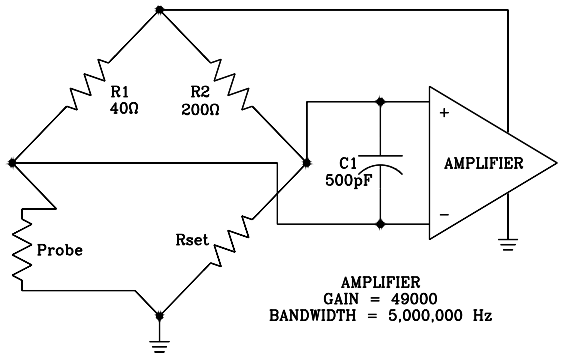

Figure 5. Simulated circuit design for conventional anemometer.

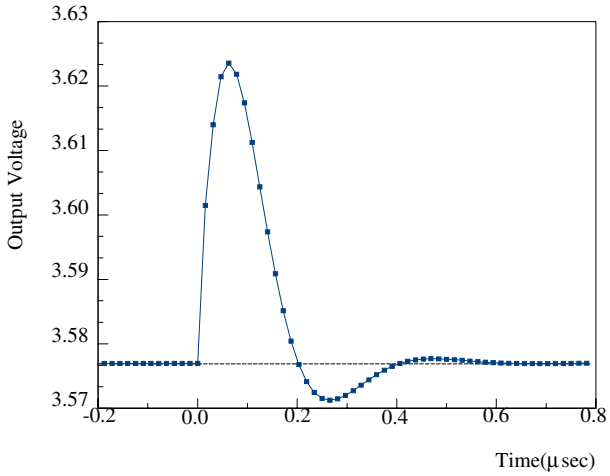

Figure 6. Impulse response of the modelled conventional anemometer.

of electronic technology, and provides a modelled system in which only the thermal effects on the frequency response are considered.

3.2. Pulse-width-modulated CTA model

The PWM-CTA is a digital electronic control system invented at Michigan State University and described in Hicks *et al* (1997) and Foss *et al* (1996). An overview of the device, whose circuit is presented in figure 7, will be given here. The operating principle of this device is to periodically heat the wire to the proper overheat temperature, followed by a cooling period during which the resistance of the sensor decreases to nominally 99% of the proper overheat value (R_{hot}). The essential components are the comparator, the master clock, a 'flip-flop', and the current source connected to the circuit at point 'E_A'. A timing diagram is shown in figure 8. The master clock triggers the flip-flop at time t_k, which applies a heating current to the sensor. The sensor temperature and resistance increase, thereby increasing the voltage at point 'E_B'. This voltage (E_B) and a reference voltage (E_{ref}) are the inputs to the comparator. When $E_B > E_{ref}$, the comparator triggers the flip-flop to turn off the heating current. This is shown as time: $t_k + \tau_k$ in figure 8. The wire will cool until the master clock initiates another heating cycle at time $t_{k+1} = t_k + \langle T \rangle$. The wire is heated again until it reaches the proper overheat resistance. This is shown as time $t_{k+1} + \tau_{k+1}$. The time duration

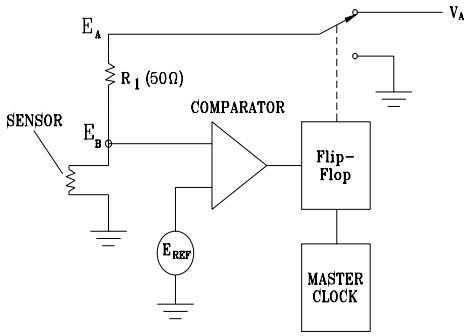

Figure 7. Circuit diagram for the PWM-CTA.

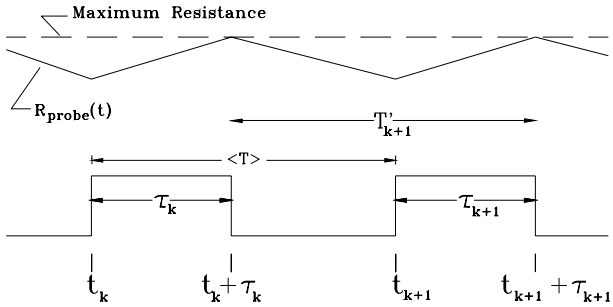

Figure 8. Timing diagram for PWM anemometer.

that current is applied to the sensor (τ_{k+1} for this cycle) is the output from the device. In a physical unit, a second high speed counter that is synchronized with the master clock measures this time duration and outputs the τ values directly to computer memory.

The electrical energy delivered to the wire during a clock cycle is represented by the ratio of the pulse width τ_{k+1} to the time $T'_{k+1} = \langle T \rangle + \tau_{k+1} - \tau_k$. This (τ/T') value is used to represent the net heat transfer from the wire given that the average temperature, or energy, of the wire is the same at times $(t_k + \tau_k)$ and $(t_{k+1} + \tau_{k+1})$. The resulting relationship between the PWM-CTA output and the cooling velocity over the wire is a second power $(\tau/T' \sim V^n)$ and not a fourth power response. The latter is characteristic of the C-CTA $(E^2 \sim V^n)$ since n is nominally 0.45. These (τ/T') data are then post processed into a time series representation of the analog velocity.

There are several advantages to the PWM method of controlling the sensor temperature. Firstly, because the system operates as an energy balance, the system should be able to track the fluid velocity for every clock cycle. That is, there is no exponential decay time and overshoot as with linear control system responses. The effective 'frequency response' is only limited by the choice of clock frequency (i.e., the resolution with which τ can be determined) and the ability of the circuit to accurately determine $E_B > E_{ref}$ in the presence of electronic noise. Physical PWM-CTA units have used a 64 kHz clock cycle for T at the time of this work. A 500 kHz system has also been utilized. Other advantages of the PWM include the potential for reduced noise levels given the absence of the high gain amplifier, increased sensitivity and stability for high speed measurements, and direct digital acquisition (no A/D required).

The simulation algorithm for the PWM-CTA was as follows. A computational loop was created which periodically

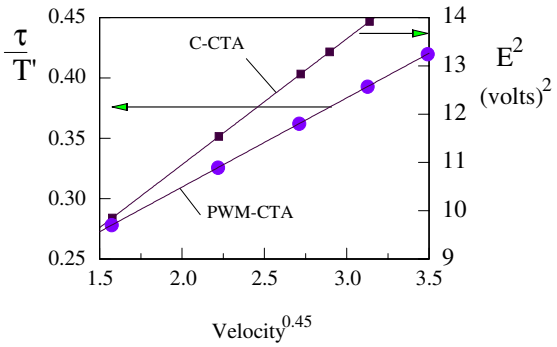

Figure 9. Calibration results for C-CTA and PWM-CTA.

Table 1. Calibration results ($2 < V < 12$ m s^{-1}).

	A	B	n
PWM-CTA simulation	0.192	0.113	0.45
Typical PWM-CTA experimental values	0.25	0.1	0.45
C-CTA Simulation	5.740	2.607	0.45
Typical C-CTA experimental values	6	3	0.45

applied the heating current in equation (2). Once the total resistance of the wire reached the overheat value of $1.7R_{cold}$ the current was set to zero for the remainder of the cycle. The time discretization of $\Delta t = 15.6$ ns was used corresponding to 1000 time steps per heating cycle. Smaller time steps were found to cause less than a 0.05% change in the output values.

4. Results of transient response

4.1. Model calibration

Both the PWM-CTA and the C-CTA models were calibrated using a range of steady state input velocity values. The simulations were run for a sufficiently long time to achieve a steady state output. The calibration results were then used to find the coefficients of the transfer functions:

$$\frac{\tau}{T'} = A_{PWM} + B_{PWM}V^n \tag{9}$$

and

$$E^2 = A_C + B_C V^n \tag{10}$$

for the PWM-CTA and the idealized C-CTA respectively. These data are shown in figure 9 with the fitted equations (9) and (10). The simulation coefficients are shown in table 1 along with values typically found in physical calibrations. The slope (B) and exponent (n) agree quite well for both simulations, indicating that the heat transfer model is reasonable. The offset term (A) was found to be somewhat lower than the A values for the physical calibrations. This is attributed to electrical components that are specific to the physical anemometers. Note that changing the constants in the heat transfer relationship given in equation (5) results in changes in the A, B, and n values of equations (9) and (10). However, these differences did not effect the transient results presented herein.

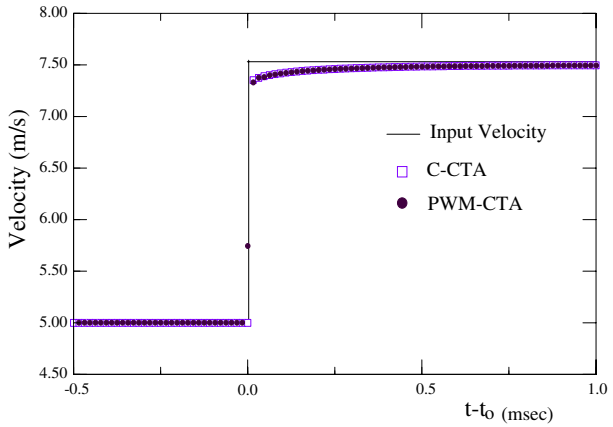

Figure 10. Anemometer output from step input velocity.

4.2. Step function response

The response of the thermal system was investigated by applying a known input velocity function through equation (5) and observing the output of the simulation. It was decided that a steady state condition ($V = 5$ m s^{-1}) followed by a step increase in velocity would provide the greatest insight into the thermal characteristics of the sensor. The frequency response will be discussed in the following section.

The data presented below were generated by the use of a step function in the input convection velocity:

$$V(t) = 5.0 + 2.5H(t - t_o)(\text{m s}^{-1}) \tag{11}$$

where $H(t - t_o)$ is the unit Heaviside step function ($H = 0$ for $t < t_o$ and $H = 1.0$ for $t > t_o$). The results from this input function for both PWM-CTA and C-CTA are shown in figure 10. These data show that both electrical control systems showed a 2.33 m s^{-1} rise in output velocity in the first 16 μs (one PWM time step) following the 2.5 m s^{-1} step in input velocity. This initial jump in output was then followed by a relatively long (∼1.0 ms) rise to the steady state velocity. Figure 11 is an expanded view of the same data using a log scale for the time axis. The linear portion of this rise to the steady state value indicates that the response is exponential where the slope is proportional to the time constant of the response.

The thermal mechanism which leads to the inability of the hot-wire to provide accurate velocity readings with transient convection velocity was described qualitatively in the discussion following equation (1). The remainder of this section will serve to clarify the exact nature of the thermal transient response. The under predicted velocity (for $0 < t < 1$ ms) presented in figure 10 can be explained as follows for the PWM-CTA. A similar argument can be presented for the C-CTA. Consider the energy balance of the sensor for a single time cycle as shown in figure 8, i.e., integrating equation (2) over the time duration $(t_k + \tau_k)$ to $(t_{k+1} + \tau_{k+1})$;

$$\rho c A_c(\Delta x)\int_{(t_k+\tau_k)}^{(t_{k+1}+\tau_{k+1})}\left[\int_{x=0}^{x=L/2}\left(\frac{\partial T}{\partial t}\right)\mathrm{d}x\right]\mathrm{d}t$$
$$= \int_{(t_k+\tau_k)}^{(t_{k+1}+\tau_{k+1})} q_{axial}\left(x = \frac{L}{2}\right)$$
$$+ \left[\int_{x=0}^{x=L/2}\{(q_{radial}) + (I^2R)\}\,\mathrm{d}x\right]\mathrm{d}t. \tag{12a}$$

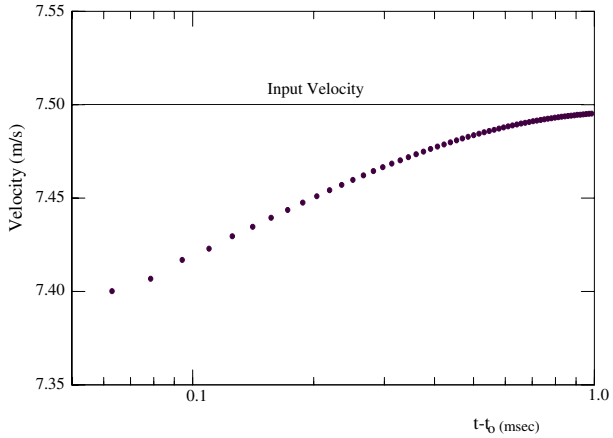

Figure 11. Expanded view of step response.

The time and spatial integrations can be interchanged on the left-hand side of the equation such that it represents the difference in the total thermal energy of the wire at the beginning and the end of a heating cycle. Because the resistance of the wire is the same at the beginning and end of a cycle, the average temperature must be the same. Therefore the net 'energy change' of the wire must be zero. Equation (12*a*) can be restated as:

$$\text{Net energy change} = 0 = \text{net conduction} + \text{convection} + \text{heating}. \qquad (12b)$$

The 'heating' as represented by τ/T' must balance the thermal energy transferred from the wire through 'conduction' and 'convection'.

It is now instructive to compare the terms of equation (12) for two heating cycles:

(i) the cycle immediately after the step function occurred, and
(ii) the cycle at the final steady state value.

In these two cases the magnitude of the convective cooling is identical (the cooling velocity is the same, and the average wire temperature is constant). In order for the net heating to be different for the two cases as indicated by the different output (velocity) values, the net conduction must be different. That is, changes in the net conduction following the step change in velocity cause the balance between the terms in equation (12) to vary compared to the steady state condition.

It is therefore instructive to examine the magnitude of conduction relative to the convection during the step response. This ratio is defined as:

$$q^* = \frac{\text{net conduction}}{\text{net convection}} = \frac{A_c(k_{\text{Tu}})\frac{\partial T}{\partial x}|_{x=L/2}}{Nuk_f\pi(L/2)(0.7T_{gas})}. \qquad (13)$$

The step function response of this heat loss ratio is shown in figure 12. The constant value for $t - t_o < 0$ indicates the steady temperature distribution preceding the step change in velocity. The response for $t - t_p > 0$ is an exponential rise similar to that shown in the simulation output. The difference between the steady state conduction at these two velocities is 2%.

A physical explanation as to why the conduction term increases with velocity is offered as follows. Increasing the convective cooling over the sensor leads to a temperature

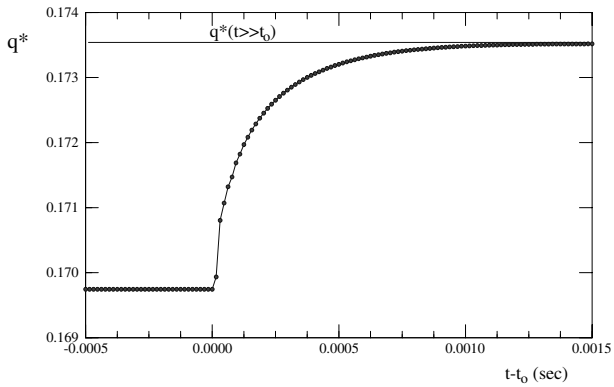

Figure 12. Dimensionless conduction from the hot-wire; see equation (14).

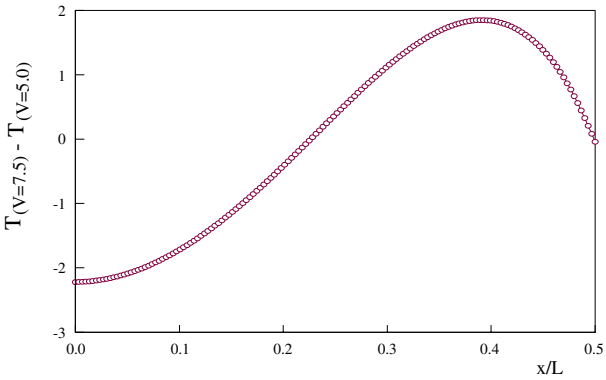

Figure 13. Steady state temperature difference from $V = 5.0$ to 7.5 m s^{-1}.

distribution along the sensor which exhibits lower temperatures in the middle region of the wire, and higher temperatures near the end of the wire. That is, the temperature distribution at higher velocities appears 'flatter' as shown schematically in figure 2. The actual difference between $T(x)$ at the two velocities 5.0 and 7.5 m s^{-1} is shown in figure 13. This flattened distribution results in a temperature gradient at $x/L = 0.5$ which increases with increasing velocity.

The calibration of a hot-wire system, either physical or numerical, is based on the steady state 'balance' of equation (12). In a transient environment, it is expected that instantaneous changes in the convective cooling will be reflected in the sensor heating (i.e., the 'output'). However, it has been shown that the conduction term does vary with velocity, and can 'disrupt' the balance in a highly transient environment. The response time of the conduction term depends on how quickly the $T(x)$ distribution can adjust to the new convective boundary condition, as discussed in the following section.

4.3. Thermal frequency response of the sensor

The thermal frequency response of the sensor was identified by using sinusoidal input functions for the cooling velocity. These tests were conducted in the range $1 < f < 2.5 \times 10.6$ (Hz). The sampling frequency was at least 50 times the input frequency in all cases in order to eliminate aliasing errors. The amplitude of the velocity output from the model was

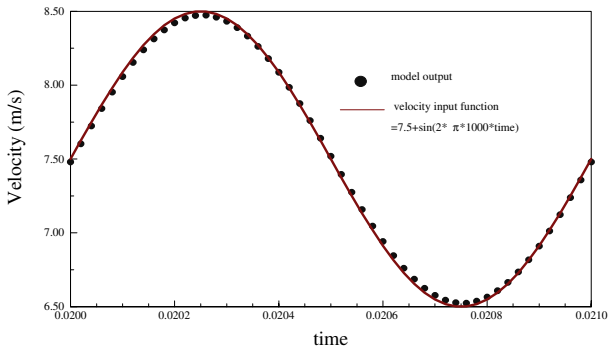

Figure 14. Example of sinusoidal input and output at 1000 Hz.

compared with the input function to determine the response ratio. Figure 14 shows an example of the input and output functions at 1000 Hz with unit magnitude. These data clearly show that the output of the anemometer underpredicts the magnitude of the sine wave input function. The response ratio (ϕ) is defined as the RMS of the output signal divided by the RMS of the input signal.

The ϕ values from these tests are shown in figure 15. The frequency is shown in Hz on the lower axis, and as a dimensionless frequency $f^* = f\tau_{thermal}$ on the upper axis, where $\tau_{thermal}$ is defined as:

$$\tau_{thermal} = \frac{4L^2}{\pi^2\alpha}. \tag{14}$$

This represents the exponential time constant of the first eigenmode of the series solution of the one-dimensional conduction–convection problem of a finite cylinder; see Ozisik (1980). For the sensor considered here, $\tau_{thermal} = 11.8$ ms. The calculated data show a unit response for the range $f < 100$ Hz. Higher frequencies show a reduced output/input amplitude ratio. Note that significant deviations from unity are observed starting near $f^* \approx 1$. The ϕ values were found to decrease throughout the range of frequencies tested, although the decreasing slope indicates that an asymptotic value will be reached in the limit $f \to \infty$. Note that no detectable phase shift was found in the computations, and therefore no phase data are presented to complement the $\phi(f^*)$ data.

For the sensor geometry described, the equations in Freymuth (1979) lead to values of $\varepsilon'_\ell = 0.93$ and $f_\ell = 260$ Hz which are also shown in figure 15. The present numerical results support both of these analytical results with the specific observations that $f^*_\ell = f_\ell\tau_{thermal} = 3.06$, and the response ratio at the highest frequency measured was found to be 0.932. Note that the shape of the $\phi(f)$ function serves to clarify the Freymuth (1979) statement that $\phi \to \varepsilon'_\ell$ for $f > 100\,f_\ell$. That is, the decrease to the $\phi(f = \infty)$ value is quite gradual, and that $f > 10^4\,f_\ell$ would more accurately indicate the range for which $\phi(f) \approx \phi(f = \infty)$.

It is noteworthy that the asymptotic value of ϕ is attained at a frequency that is much larger than that which would be experienced for a typical anemometer system. Figure 15, can be used as a guide to the expected attenuation for a given measurement. As a representative example, consider that the Kolmogorov microscale is 0.15 mm for this 7.5 m s^{-1} flow speed. The corresponding frequency would be 5×10^4 Hz, where $\phi \approx 0.94$.

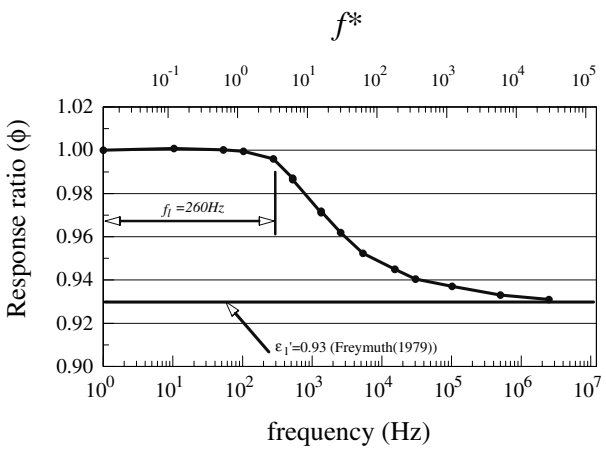

Figure 15. Thermal frequency response.

5. Conclusions

The effects of thermal transients on the output of a hot-wire system have been investigated in this numerical work. Two distinct electrical control circuits: a conventional CTA with idealized components, and a PWM-CTA, were modelled to ensure that the results were not related to the simulated electronics. A typical 5 μm diameter, 1 mm long, tungsten hot-wire was modelled. Two types of velocity input functions were used to explore the physical nature of the thermal transients. A step response was used to clarify the role of the heat conduction term in equation (12) during a change between two steady state conditions. The frequency response of the sensor $\phi(f)$ was determined by testing a range of sine wave input functions.

As confirmed by these computations, the ability of a hot-wire and its electronic control system to accurately follow the true convection velocity of the fluid depends not only on the electrical control system but also on the thermal characteristics of the hot-wire sensor. The latter dependency reflects the fact that the anemometer can only control the averaged temperature of the sensor, and, the transient changes in the distribution $T(x)$ do have an effect on the system output.

It is noted, again, that the analytical work of Freymuth (1979) clearly indicates the conclusions above. The present work serves to clarify the importance of this theory, and to document the true response of a wire without the use of simplifying assumptions. To this end, figure 15 provides a specific response ratio (ϕ) as a function of the velocity fluctuation frequency for the sensor of this study. Note that Freymuth (1979) assumes a heating ratio of 1.2 in his analysis, and then provides results which are independent of this parameter. The present computations used a heating ratio of 1.7. The agreement the Freymuth predictions and the present results confirms that the thermal frequency response is not dependent on the heating ratio. Also, several of the data points used to create figure 15 were repeated with a range of heating ratios between 1.2 and 2.0. The results from these computations showed no observable effect on the response ratio (ϕ).

The numerical code developed for the present computations can also be used to test a number of hot-wire applications where the analytical framework is not well established. For

example, the effects of parameters such as Reynolds number and the Mach number could be studies. The code developed for this work can also be used to examine the characteristics of unusual sensor configurations, such as non-constant wire diameter, or variable material properties. The use of micro-machined hot-wire sensors is a growing field in which the manufacturing options are considerably greater than conventional techniques (see, e.g., Naguib 2001). There exists the possibility to create sensors with specialized characteristics for a given application. The present numerical analysis can serve to aid in both the design of these sensors, and in the interpretation of acquired data.

In closing, it is noted that a complete understanding of the electronic control system (see, e.g., Freymuth 1977) as well as the transient thermal effects should be considered when working with experimental data in which high frequency response is required. An impulse function in the voltage applied to the wire (i.e., the familiar square wave test for a C-CTA) is a typical method to determine the response characteristics of the feed-back control system. This information must be combined with the thermal effects of a hot-wire for a complete understanding of the system's transient response capability.

References

Bruun H H 1995 *Hot-Wire Anemometry–Principles and Signal Analysis* (New York: Oxford University Press)

Comte-Bellot G 1976 Hot-wire anemometry *Annu. Rev. Fluid Mech.* **8** 209–31

Comte-Bellot G 1998 *Handbook of Fluid Mechanics* (Boca Raton, FL: Chemical Rubber Company Press)

Foss J F, Bohl D G and Hicks T J 1996 The pulse width modulated-constant temperature anemometer *Meas. Sci. Technol.* **7** 1388–95

Freymuth P 1977 Frequency response and electronic testing for constant-temperature hot-wire anemometers *J. Phys. E: Sci. Instrum.* **10** 705–10

Freymuth P 1979 Engineering estimate of heat conduction loss in constant temperature thermal sensors *TSI Quart.* **4** 3–6

Hicks T J, Foss J F and Bohl D G 1997 Pulse width modulated constant temperature anemometer *US Patent Specification* 5,654,507

Incropera F and DeWitt D 1990 *Introduction to Heat Transfer* (New York: Wiley)

Naguib A 2001 *The MEMS Handbook* ed M Gad-el-Hak (Boca Raton, FL: Chemical Rubber Company Press) ch 23

Ozisik M 1980 *Heat Conduction* (New York: Wiley)

Perry A E 1982 *Hot-Wire Anemometry* (New York: Oxford University Press)

Thomas R E and Rosa A J 2001 *The Analysis and Design of Linear Circuits* (Englewood Cliffs, NJ: Prentice-Hall)